

Applying Palmprint Feature Vector on Hand Lines Recognition System

**Assistant Lecturer Imad A.Rasool A.
University of Technology**

1. Introduction

Biometric has gained much attention in the security world recently. Many types of personal authentication systems have been developed, and palm print verification is one of the emerging technologies [1].

Palmprint is considered one of the significant biometric identifiers because it is unique, stable for a long time period, rich of features. Palmprint may be defined as the inner surface of the hand between the fingers and the wrist. The palm richness of extractors comes from the features found in it which are principal lines, wrinkles, ridges, datum points [2].

This paper describes the main work performed in this system. Our research is composed of many stages which are palmprint acquisition, preprocessing stage, feature extraction stage until matching with result stored in a feature vector. Fig(1) is a simplified block diagram of the proposed system. Our palm images are captured using traditional scanner device with resolution of 150 dpi (Dot Per Inch) and Fig(3) shows a general flowchart of this work.

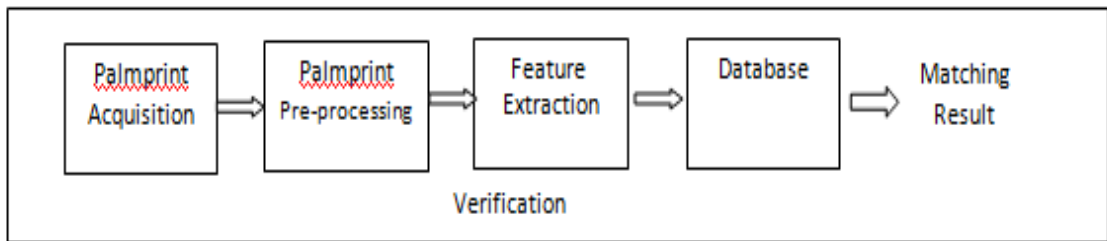


Fig (1) system design stages

2. System Design

The proposed system is composed of many stages as it is seen in Fig(3) and these stages include acquisition of the palm which is performed using traditional scanner, the preprocessing stage, and the feature extraction stage and the template storage.

2.1 Preprocessing

This part deals with the Orientation of the captured palm image, the Region Of Interest (ROI) selection, and resizing the image to a standard predefined scale which is 400x400 pixel and finally converting the colored image to gray scale. Fig (2) shows two images of palm print before and after the preprocessing stage.

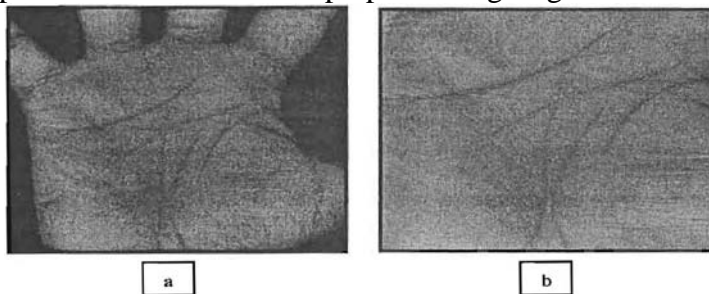


Fig (2) a) entered image b) image ready for processing

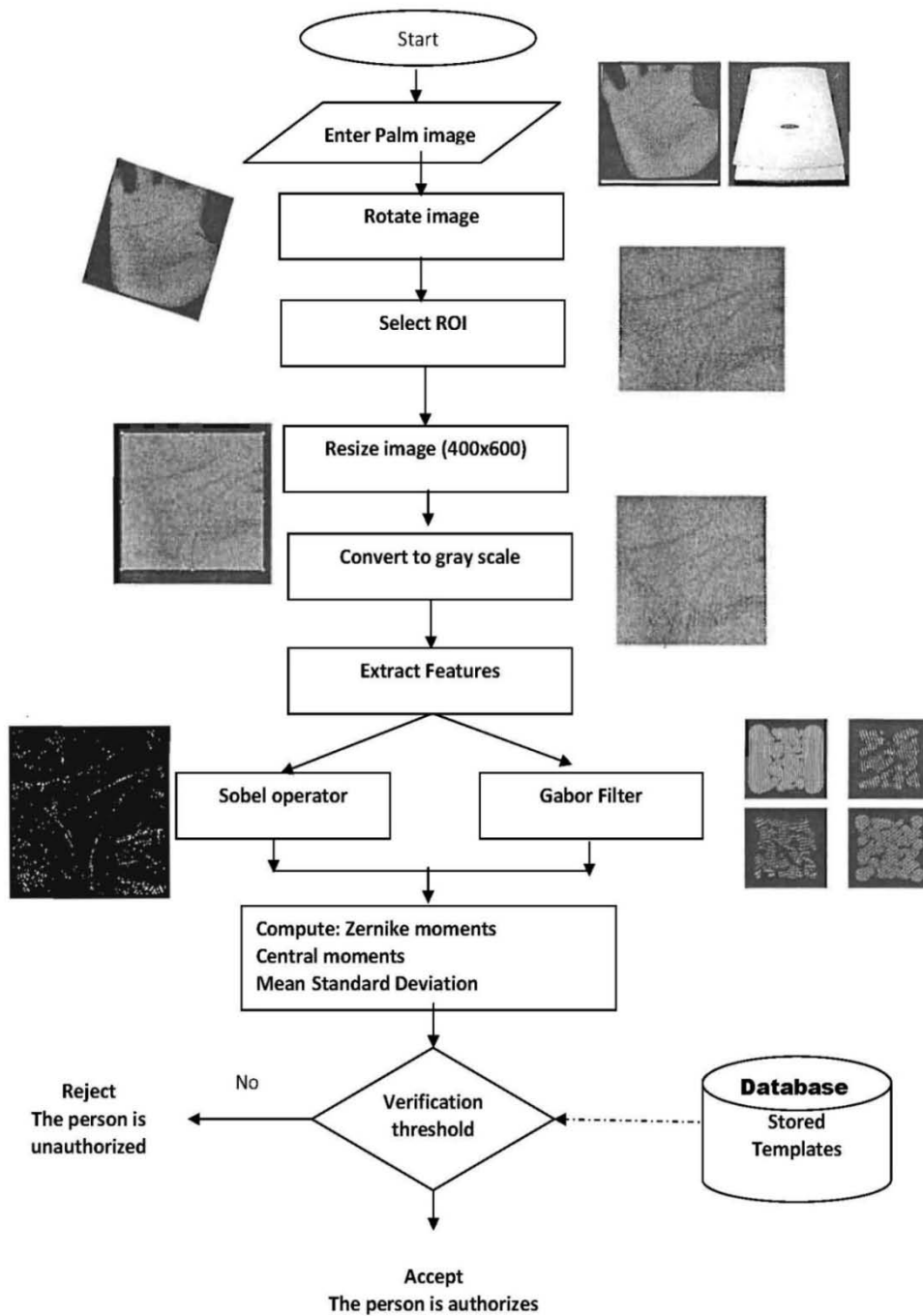


Fig (3) General Flowchart of the proposed system

2.2 Feature extraction

Feature extraction plays an important role in image identification and verification. There are many features exhibited in the palm [3].

Our feature extraction is composed of multiple feature extraction methods they are

- Gabor Filter
- Sobel Edge Detector

Each one of these filters is applied separately on the preprocessed image and then for each output the following measures are computed

- Zernike Moments
- Traditional Moments
- Mean
- Standard Deviation

Fig (4) shows the feature extraction module of our proposed system.

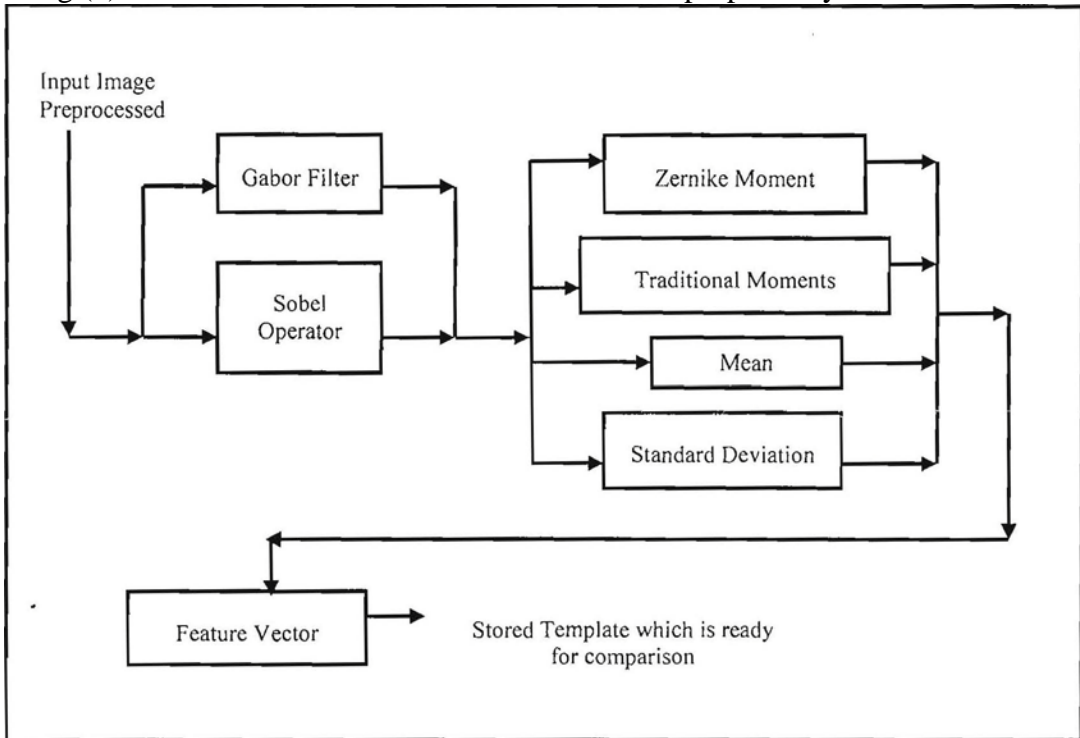


Fig (4) The Feature Extraction Module

2.2.1 Gabor Filter

Gabor filter, Gabor filter bank, Gabor transform and Gabor wavelet are widely applied to image processing, computer vision and pattern recognition. This function can provide accurate time-frequency location governed by the "Uncertainty Principle". A circular 2-D Gabor filter in the spatial domain has the following general form:

$$G(x,y,\theta,u,\sigma) = \frac{1}{2\pi\sigma^2} \exp\left\{-\frac{x^2 + y^2}{2\sigma^2}\right\} \exp\{2\pi i(ux \cos \theta + uy \sin \theta)\} \dots\dots (1)$$

Where $i = \sqrt{-1}$; u is the frequency of the sinusoidal wave; θ controls the orientation of the function and σ is the standard deviation; and x, y will determine the size of the applied filter. Such Gabor filters have been widely used in various applications. In addition to accurate time-frequency location, they also provide robustness against varying brightness and contrast of images. Furthermore, the filters can model the

receptive fields of a simple cell in the primary visual cortex. Based on these properties, in this work, we tried to apply a Gabor filter to palmprint authentication [2] Fig (5) shows the output of the entered palm image i.e. after preprocessing.

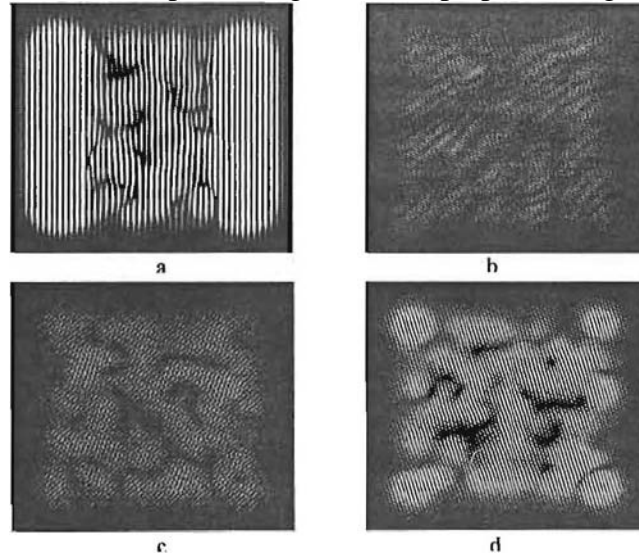


Fig (5) Gabor filter in four angle values

a)0°, b)45°, c)90°, d)135°

2.2.2 Sobel Operator

The Sobel operator performs a 2-D spatial gradient measurement on an image and so emphasizes regions of high spatial frequency that correspond to edges. Typically it is used to find the approximate absolute gradient magnitude at each point in an input grayscale image. In theory at least, the operator consists of a pair of 3x3 convolution kernels as shown in the two masks. One kernel (mask) is horizontal and the other rotated by 90° (vertical)[4] [5].

**Column
Mask**

-1	-2	-1
0	0	0
1	2	1

**Row
Mask**

-1	0	1
-2	0	2
1	0	1

These masks are each convolved with the image. At each pixel location we now have two number; s_1 , corresponding to the result from the row mask, and S_2 , from the column mask. We use these numbers to compute two metrics, the edge magnitude and the edge direction, which are defined as follows:

$$\text{Edge Magnitude} = \sqrt{S_1^2 + S_2^2} \dots\dots\dots (2)$$

$$\text{Edge Direction} = \tan^{-1} \left[\frac{S_1}{S_2} \right] \dots\dots\dots (3)$$

The edge direction is perpendicular to the edge itself because the direction specified is the direction of the gradient, along which the gray levels are changing [4][5] Fig (6) shows output of sobel.



Fig (6) Sobel operator output image

2.2.3 Zernike Moments

The kernel of Zernike moments is a set of orthogonal Zernike polynomials defined over the polar coordinate space inside a unit circle. The two dimensional Zernike moments of order p with repetition q of an image intensity function $f(r, \theta)$ are defined as:

$$Z_{pq} = \frac{P+1}{\pi} \int_0^{2\pi} \int_0^1 V_{pq}(r, \theta) f(r, \theta) r dr d\theta ; |r| \leq 1 \dots\dots\dots (4)$$

Where Zernike polynomials $V_{pq}(r, \theta)$ are defined as:

$$V_{pq}(r, \theta) = R_{pq}(r) e^{jq\theta} ; j = \sqrt{-1} \dots\dots\dots (5)$$

and the real-valued radial polynomials, $R_{pq}(r)$, is defined as follows:

$$R_{pq}(r) = \sum_{k=0}^{\frac{p-|q|}{2}} (-1)^k \frac{(p-k)!}{k! \left(\frac{p+|q|}{2} - k \right)! \left(\frac{p-|q|}{2} - k \right)!} r^{p-2k} \dots\dots\dots (6)$$

where $0 \leq |q| \leq p$ and $p - |q|$ is even.

If N is the number of pixels along each axis of the image, then the discrete approximation Of equation (4) is given as:

$$Z_{pq} = \lambda(p, N) \sum_{i=0}^{N-1} \sum_{j=0}^{N-1} R_{pq}(r_{ij}) r_{ij}^{-jq\theta_j} f(i, j); 0 \leq r_{ij} \leq 1 \dots\dots\dots (7)$$

where $\lambda(P, N)$ is normalizing constant and image coordinate transformation to the interior

of the unit circle is given by

$$r_y = \sqrt{x_i^2 + y_j^2}; \theta = \tan^{-1} \left(\frac{y_j}{x_i} \right); x_i = c_1 i + c_2; y_j = c_1 j + c_2; \dots\dots\dots (8)$$

And $\lambda(P, N)$ is computed as follows:

$$\lambda(p, N) = \frac{4(p-1)}{(N-1)^2 \pi}; c_1 = \frac{\sqrt{2}}{N-1}; c_2 = \frac{-1}{\sqrt{2}} \dots\dots\dots (9)$$

ff

Therefore,

$$x_i = \frac{\sqrt{2}}{N-1} i + \frac{-1}{\sqrt{2}} \text{ and } y_j = \frac{\sqrt{2}}{N-1} j + \frac{-1}{\sqrt{2}} \dots\dots\dots (10)$$

This implementation, is for square image ($N \times N$) and normalized over a unit circle [6][7].

2.2.4 Traditional Moments

These moments are also named orthogonal moments. For a 2-D continuous function $f(x, y)$ of order $(p+q)$ is defined as

$$m_{pq} = \int_{-\infty}^{\infty} \int_{-\infty}^{\infty} x^p y^q f(x, y) dx dy \dots\dots\dots (11)$$

For $p, q = 0, 1, 2, \dots$

A uniqueness theorem states that if $f(x, y)$ is piecewise continuous and has non zero values only in a finite part of xy plane, moments of all order exist and the moment sequence (m_{pq}) is uniquely determined by $f(x, y)$. Conversely, (m_{pq}) uniquely determines $f(x, y)$. The central moments can be expressed as

$$\mu_{pq} = \int_{-\infty}^{\infty} \int_{-\infty}^{\infty} (x - \bar{x})^p (y - \bar{y})^q f(x, y) dx dy \dots\dots\dots (12)$$

$$\text{where } \bar{x} = \frac{m_{10}}{m_{00}} \text{ and } \bar{y} = \frac{m_{01}}{m_{00}}$$

For a digital image, Eq.(12) becomes

$$\mu_{pq} = \sum_x \sum_y (x - \bar{x})^p (y - \bar{y})^q f(x, y) \dots\dots\dots (13)$$

which are

$$\mu_{00} = m_{00} \quad \mu_{10} = 0$$

$$\mu_{01} = 0$$

$$\mu_{11} = m_{11} - \bar{y}m_{10} \quad \mu_{20} = m_{20} - \bar{x}m_{10}$$

$$\mu_{02} = m_{02} - \bar{y}m_{01}$$

$$\mu_{10} = m_{30} - 3\bar{x}m_{20} + 2\bar{x}m_{10} \quad \mu_{12} = m_{12} - 2\bar{y}m_{11} - \bar{x}m_{02} + 2\bar{y}^2 m_{10}$$

$$\mu_{21} = m_{21} - 2\bar{x}m_{11} - \bar{y}m_{20} + 2\bar{x}^2 m_{01}$$

$$\mu_{03} = m_{03} - 3\bar{y}m_{02} + 2\bar{y}^2 m_{01}$$

The normalized central moments, denoted η_{pq} , are defined as

$$\eta_{pq} = \frac{\mu_{pq}}{\mu_{00}^\gamma} \dots\dots\dots (14)$$

where

$$\gamma = \frac{p+q}{2} + 1 \dots\dots\dots (15)$$

A set of seven invariant moments can be derived from the second and third moments [2]:

$$\phi_1 = \eta_{20} + \eta_{02} \dots\dots\dots (16)$$

$$\phi_2 = (\eta_{20} - \eta_{02})^2 + 4\eta_{11}^2 \dots\dots\dots (17)$$

$$\phi_3 = (\eta_{30} - 3\eta_{12})^2 + (3\eta_{21} - \eta_{03})^2 \dots\dots\dots (18)$$

$$\phi_4 = (\eta_{30} + 3\eta_{12})^2 + (3\eta_{21} + \eta_{03})^2 \dots\dots\dots (19)$$

$$\phi_5 = (\eta_{30} - 3\eta_{12})(\eta_{30} + \eta_{12})[(\eta_{30} + \eta_{12})^2 - 3(\eta_{21} + \eta_{03})] + (3\eta_{21} - \eta_{03})(\eta_{21} + \eta_{03})[3(\eta_{30} + \eta_{12})^2 - (\eta_{21} + \eta_{03})^2] \dots\dots\dots (20)$$

$$\phi_6 = (\eta_{20} - \eta_{02})[(\eta_{30} + \eta_{12})^2 - (\eta_{21} + \eta_{03})^2] + 4\eta_{11}(\eta_{30} + \eta_{12})(\eta_{21} + \eta_{03}) \dots\dots\dots (21)$$

$$\phi_7 = (3\eta_{21} - \eta_{03})(\eta_{30} - \eta_{12})[(\eta_{30} + \eta_{12})^2 - (\eta_{21} + \eta_{03})^2] + (3\eta_{12} - \eta_{30})(\eta_{21} - \eta_{03})[3(\eta_{30} + \eta_{12})^2 - (\eta_{21} + \eta_{03})^2] \dots\dots\dots (22)$$

This set of moments is invariant to translation, rotation, and scale change [5].

2.2.5 Mean and Standard Deviation

A-Mean: Average or mean value computes the mean of a set of elements (the sample

$$\text{average } \bar{x} = \frac{1}{n} \sum_{i=1}^n x_i \dots\dots\dots$$

... (23)

where n is the number of elements in the given set, X_i defines the set elements [5][6].

B-Standard Deviation: This computes the standard deviation of the data of a sample.

$$\delta = \sqrt{\frac{1}{n-1} \sum_{i=1}^n (x_i - \bar{x})^2} \dots (24)$$

where \bar{x} is the sample average. Standard Deviation normalizes by $n-1$ where n is the sequence length [5][6].

3. Implementation

Here one can see implementation of the different stages of the proposed system. Fig (2.a) shows first the entered image and Fig (2.b) shows the image after preprocessing that is ready for feature extraction.

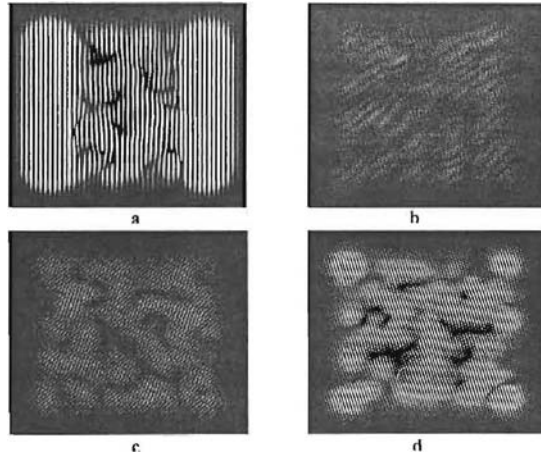


Fig (7) Implementation of Gabor filter in four angle values
a)0°, b)45°, c)90°, d)130°



Fig (8) Sobel operator output image

Measures		G0	G45	G90	G135	S
Zernike		11.2157- 0.4125i	0.1878- 1.9893i	-3.4553- 3.1904i	5.4390- 3.9645i	-0.0092- 0.0080i
Orthogonal Moments	01	0.3372	0.3373	0.3353	0.3387	7.3806
	02	4.9663×10^4	7.7536×10^{-6}	1.8374×10^{-5}	1.1527×10^{-5}	1.5745
	03	1.1499×10^{-5}	3.0281×10^{-6}	4.1455×10^{-5}	4.6612×10^{-6}	4.1629
	04	4.1639×10^{-7}	1.9301×10^{-6}	1.1523×10^{-6}	6.5597×10^{-8}	8.0215
	05	-5.0834×10^{-14}	-4.2724×10^{-12}	7.1703×10^{-12}	-1.1237×10^{-14}	10.8715
	06	6.3169×10^{-9}	5.3230×10^{-9}	-4.9375×10^{-9}	-6.2848×10^{-11}	-2.1996
	07	3.3924×10^{-13}	1.6927×10^{-12}	2.2141×10^{-13}	1.2996×10^{-14}	-48.3101
Mean		66.8662	16.1806	23.9233	34.1745	0.0278
Standard Deviation		102.3557	34.4121	49.9603	49.9603	0.1643

Table (1) the output measures for one hand

Table (1) shows the feature vector of one entered palm image. These values are produced for five intermediate images which are the resultants of Gabor implementation and Sobel implementation. Gs' define the Gabor output for the four angles 0°, 45°, 90°, 135°, respectively and S defines the output of Sobel. This means that each feature vector contains 50 values, one complex value for Zernike moments, seven values for orthogonal moments, two values for mean and standard deviation.

4. Conclusions

The proposed system produces a feature vector that contains a lot of information for each sample. This will increase the chance of true identification / verification for an individual rather than using one or two values. These feature extractors vary in their responses so if one value is diverging it will not have too much effect when the other values are converging i.e. the error rate is little. The proposed system~as shown in Fig(3) shows two different processes for feature extraction one depending on Gabor filter and-the other depends on the Sobel Operator.

References

- [1] Tee Connie, Andrew Teoh, "**Palmprint Recognition with PCA and ICA**", Faculty of Information Sciences and Technology, Multimedia University, Melaka, Malaysia (2003)
- [2] Zhang David, Kong Wai-Kin, "**Online Palmprint Identification**", IEEE Pattern Analysis and Machine Intelligence, Vol.25, No.9, September 2003.
- [3] You Jane, Li Wenxin, "**Hierarchical Palmprint Identification via multiple feature extraction**", The Journal of the Pattern Recognition 35 (2002) 847-859
- [4] Umbaugh Scott E, "**Computer Vision and Image Processing CVIP**", Published by Prentice Hall PTR, United States of America (2000),
- [5] Rafael C. Gonzales, Richard E. Woods, "**Digital Image Processing**", Published by Addison Wesley Longman (Singapore) Pte Ltd (2000).
- [6] Paug Ying-Han, Andrew T. B. 1., "**Palmprint Verification with Moments**", Journal of WSCG, Vol.12, No.1-3, WSCG 2004, February 2-6, 2003, Plzen, Czech Republic.
- [7] Simon X. Liao and Mirosław Pawlak, "**On the Accuracy of Zernike Moments for Image Analysis**", IEEE Transactions on Pattern Analysis And Machine Intelligence, VOL. 20, No. 12, December 1998